Electronic Supplementary Information

Proton Selective Adsorption on Pt-Ni Nano-thorn Array Electrodes for Superior Hydrogen Evolution Activity

Adeela Nairan, ‡ [a] Caiwu Liang, ‡ [a] Sum-Wai Chiang, [a] Yi Wu, [b] Peichao Zou, [a] Usman Khan, [c] Wendong Liu, [b] Feiyu Kang, [a] Shaojun Guo, [d] Jianbo Wu* [b,e,f], Cheng Yang* [a]

a. Institute of Materials Research, Tsinghua Shenzhen International Graduate School, Tsinghua University, Shenzhen 518055, China.

b. State Key Laboratory of Metal Matrix Composites, School of Materials Science and Engineering, Shanghai Jiao Tong University, 800 Dongchuan Road, Shanghai 200240, China.

c. Shenzhen Geim Graphene Center, Tsinghua-Berkeley Shenzhen Institute, Tsinghua University, Shenzhen 518055, China

d. College of Engineering, Peking University, No.5 Yiheyuan Road, Haidian District, Beijing, 100871, China.

e. Center of Hydrogen Science, Shanghai Jiao Tong University, 800 Dongchuan Road, Shanghai 200240, China;

f. Materials Genome Initiative Center, Shanghai Jiao Tong University, 800 Dongchuan Road, Shanghai 200240, People's Republic of China.

‡ These authors contributed equally

Email: yang.cheng@sz.tsinghua.edu.cn
Email: jianbowu@sjtu.edu.cn

Supplementary Note 1

Experimental Details

1. Chemicals

Nickel chloride hexahydrate ($NiCl_2 \cdot 6H_2O$), chloroplatinic acid hexahydrate ($H_2PtCl_6 \cdot 6H_2O$), hydrazine monohydrate ($N_2H_4 \cdot H_2O$), trisodium citrate dihydrate ($Na_3C_6H_5O_7 \cdot 2H_2O$), and potassium hydroxide (KOH) were all purchased from Alfa Aser. All the chemicals were used as-received without any further purification.

2. Fabrication of Ni nano-thorn arrays (Ni NTAs)

In a typical preparation of Ni NTAs, Ti foil (thickness 40 μm) was used as a substrate. Ti foil was cleaned ultrasonically in 3M HCl to remove the surface oxide layer, and then washed with deionized water and dried in an oven at 60 ℃ for 2 h. Then the Ni NTAs were deposited onto the substrate using a magnetic field driven growth process. Primarily, a 100 mL aqueous solution of 0.1M $NiCl_2 \cdot 6H_2O$ and 37mM $Na_3C_6H_5O_7 \cdot 2H_2O$ was prepared. Then, the same amount of ion exchange water containing 0.5M $N_2H_4 \cdot H_2O$ was also prepared. The pH of both solutions was adjusted by 6M KOH using a pH meter (HORIBA, F-71) to 12. The prepared solutions were bubbled by nitrogen gas to remove the dissolved oxygen. Ti foil was attached vertically inside a beaker, consisting of both solutions and a magnetic field was applied up to 5 kilo-Gauss by a Helmholtz coil (Eastern Morning View EM7). To get more insight into the morphology of the fabricated nanothorn arrays, temperature-controlled experiments were carried out ranging from 60-100 ℃. Those Ni NTAs fabricated at 80 ℃ showed a typical NT structure on the surface of nanowires, after 1 h reaction time. The Ni NTAs were washed several times with deionized water and ethanol and dried in a desiccator. The control sample of smooth Ni nanowire arrays (Ni NWAs) was prepared with the same treatment except the temperature was kept 65 ℃. The average mass loading of as-prepared electrodes was about 1.5 mg cm^{-2}.

3. Preparation of Pt-Ni NTAs

The Pt-Ni NTAs were fabricated via chemical electrodeposition using work station CH660E. Before electrodeposition, an aqueous solution containing 0.5M H_2SO_4 and 4mM $H_2PtCl_6 \cdot 6H_2O$ was prepared. The electrodeposition of Pt layer on Ni NTAs was carried out by using three- electrode configuration, where the Ni NTAs sample, graphite electrode, and

Ag/AgCl electrode were used as working electrode, counter electrode and reference electrode, respectively. During electrodeposition, a constant voltage of -0.25 V (vs Ag/AgCl reference electrode) was applied for 60 seconds. Finally, the as-prepared electrode was rinsed with deionized water to remove the impurities and dried in an oven at 60℃ for 2 hrs. The average mass loading of fabricated Pt-Ni electrodes was about 1.516 mg cm^{-2}, representing that Pt loading was only about~ 0.016 mg cm^{-2}.

4. Materials Characterization

Field emission electron microscope (FE-SEM, HITACH S4800, Japan) and transmission electron microscope (TEM, JEM 2100F) were used to examine the morphology and microstructure of the samples. For TEM measurement, samples were prepared by dispersion in the ethanol and thereafter dropping the dispersion onto a copper grid and then dried at ambient conditions. X-ray photoelectron spectroscopy (XPS, ESCALABSB 250 Xi) spectra were recorded to analyze the surface species and their chemical states. The phase and crystal structure of the as-prepared samples was determined by X-ray diffraction (XRD, Bruker DS RINT2000/PC, Germany) with Cu Kα radiation. The nanowires were peeled-off from the substrate before characterizations. The surface area of the prepared electrodes was measured by Micromeritics ASAP 2020 specific surface area analyzer. The elemental concentration of samples was analyzed by inductively coupled plasma atomic emission spectroscopy (ICP-AES-FHM22). The contact angles of gas bubbles under electrolytes were tested by the method of the captive bubble using Kruss DSA30 system. The images of hydrogen bubbles release were obtained by the camera (SONY NEX6) equipped with a macro lens.

5. Electrochemical Measurement

All electrochemical measurements were performed on an electrochemical workstation (CHI 660E, CH Instruments, China) in a three-electrode configuration at room temperature. Typically, Graphite rod (with a diameter of 8mm) and standard Ag/AgCl electrode (in 3M KCL) were used as counter and reference electrodes, respectively. Before electrochemical measurements, the electrolyte was bubbled by N_2 gas for 15 min to achieve an oxygen-free solution. For comparison, 20 wt% Pt/C was used as an HER electrocatalyst. All tests were carried out in 1M KOH solution and potential was referred versus RHE. The reference electrode was first corrected as follow: Two Pt electrodes were cleaned and cycled in 0.5 M H_2SO_4 electrolyte for 2 hours to remove the surface impurity, and employed as working

electrode and counter electrode in 1 M KOH electrolyte. The electrolyte was bubbled with H_2 over the working electrode during the calibration. A CV measurement at low scan rate of 1 mV s^{-1} were carried out to determine the zero current potential (the interconversion between the hydrogen oxidation and hydrogen evolution reaction). As shown in Figure S20, the potential of zero net current is −1.02 V versus the Ag/AgCl electrode. Thus the RHE was calculated as $E_{RHE} = EA_{g/AgCl}$ +1.02 V. The iR compensation was performed by automatic current interrupt method with a value of 95% × Ru through CH instrument 660E working station. Subsequently, catalytic activity was measured by a linear sweep voltammetry method with a scan rate of 1 mV s^{-1}. The catalyst ink was prepared by dispersion of Pt/C into a mixture of water/ethanol solution (4 : 1) and 10 μL of 5 wt% Nafion solute ion, followed by ultrasonication for 0.5 h. Later on, different amount of the catalyst solution was dropped onto the glassy carbon electrode. After being dried the electrode was used as a working electrode for the electrochemical measurements. The mass loading amount of catalysts was estimated to be about 30, 100, and 500 μg cm^{-2}. The polarization curves of Pt/C catalysts with different mass loading were recorded (Figure S21), and for better comparison, Pt/C with 500 μg cm^{-2} was used as benchmark catalysts. The double-layer capacitance (C_{dl}) was calculated by measuring the capacitive current at different scan-rate of cyclic voltammetry. The scan rates were 20, 40, 60, 80, and 100 mV sec^{-1}. The C_{dl} was estimated by plotting the $\Delta J = J_a - J_c/2$ versus scan rate. The electrochemical impedance spectra of the fabricated electrodes were carried out by AC impedance spectroscopy under the frequency range from 100 kHz to 0.1 Hz at 100 mV overpotential versus RHE. A 500 mL glassware from Gaoss Union were used as container for electrochemical test of LSV, CV and EIS. The glassware is made of borosilicate glass, which possesses better alkaline corrosion resistance ability than normal glass. Figure S22 shows the set-up of electrochemical test and the optical images of Pt-Ni NTAs samples. To eliminate the corrosion effect of the glass during test, we also recorded the XPS spectrum after the test, and not Si signal was detected (Figure S23). For long term stability test, a 150 mL PTFE container was used, and the electrolyte was bubbled with N_2 before and during the test to remove dissolved CO_2 and avoid carbonate impurities in the solution (Figure S24).

Supplementary Note 2

Numerical Simulations

1. Simulation Setup

In this work, finite element method (FEM) simulation packages ANSYS is used to analyze the electric field distribution on two Pt-Ni nanowire models with NT structures, which reflect the real surface morphology of the sample. For clear visualization of electric field generation, a control case simulation on the smooth nanowire was also carried out.

2. Reaction-Diffusion Equation for Modelling

To investigate the catalytic effect based on the electric field values, we referred to the method reported by Huijun Jiang *et al.* and their discussion is based on the reaction-diffusion equation (RDE)[1], which expresses the production rate of chemicals from reaction sources. Equation 1 is the RDE for the main product along with the field-induced extra mass transfer into the systems free-energy density functional. For a position r on the surface, the RDE is:

$$\frac{\partial\theta(r)}{\partial t} = \varphi_0(1-\theta) - k_d\theta - k\theta - k_s\theta + D^2\theta - \frac{D}{K_BT}.[\theta(1-\theta)V] \quad (1)$$

Where k_B is the Boltzmann constant, T is the temperature, D and θ are the surface diffusion coefficient and the concentration normalized by its maximal value. The first term on the right side explains the effective adsorption with the rate constant φ_0 from the solution to the electrode surface, which compact diffusion across the solution and adsorption of nearby H_2 to the electrode surface. The adsorbed hydrogen can also desorb from the surface back into the solution with a rate constant k_d. Such a pair of reversible processes determines the equilibrium surface concentration for a bare surface without any follow-up reactions. The V potential around the tip leads to extra mass transfer as compared to the other part of the nanowire surface, which is governed by the electric field U_{tip} around the tip as in equation 2:

$$V(r) = \alpha\theta U_{tip} exp\left\{-\frac{|r-r_{tip}|^2}{r_0^2}\right\} \quad (2)$$

This equation enables us to discuss the electrochemical activity by observing the electric field distribution on this unique NT geometry, and make it possible to use the electric field to reflect the overall reaction rate improvement in the experiment. Here, we assume the concentrations of relevant reactants are abundant in the electrolyte.

3. Simulation Domain and Procedure

The simulation domain consists of the region near the tip of a nanowire where electric field activity is dominant. We build a single nanowire model which shows the randomly distributed nanothorn structures on the surface of nanowire and this nanowire serves as cathode as represented in Figure S18. Due to consideration on computational complexity, we assume a domain where the nanowire is a cylinder with length and diameter of 4000 nm and 350 nm,

respectively. The whole system including electrodes and electrolytes has a dimension of 1300 nm x 1300 nm x 8000 nm (excluding the electrodes' thickness).

In order to better relate our simulation with the fabricated nanowire structure, we calculate the statistical parameters including NT base, height, and tip angles from representative SEM images (Figure S1 c, e, and Figure 1b). Using the statistics listed in Supplementary Table 3, the model is created with the Monte Carlos generation mechanism. The electrochemical conductivities in the simulation model for nanowire and NT structure is 1.43×10^7 S m^{-1}, and for KOH electrolyte is 166.6 S m^{-1}, which are referred to typical values from these materials. The electric field distribution is simulated across the electrochemical system, and then the effect of this conductive nanowire structure can be discussed quantitatively.

4. Electric-field distribution around the smooth nanowire and NTs systems

Here, we have added a model representing a 2D distribution of electric field along the nanowire with NTs and a smooth nanowire (Figure S19). In this case, we can observe that in comparison with smooth nanowire, various high Electric field spots are created along the nanowire with NTs (Figure S19b), without significantly weakening the overall high electric field distribution on the nanowire tips. This means the presence of NTs created more catalytically active sites along the nanowire surface and resultantly enhances the kinetics of the overall reaction. This simulation results strongly support the observation of better catalytic activity for thorn-like nanostructures.

Although the model we established here is only a short and vertical nanowire structure, it is sufficient to reflect the enhancement of the electric field at the tip of the NT structure. In practice, because the nanowires are very long (hundreds of micrometers or even millimeters), they will fall down, leaving a large number of nanowires with NT structures near the top of the opposite electrode. From the SEM image, we can see that the NTAs can reach tens to hundreds of microns in thickness (Figure S2), so the NT structure in the above region is less bound by the electric field of the bottom substrate, which will show a strong electric field enhancement phenomenon This concludes that the NT structure plays a dominant role to promote the electric field generation during the catalytic process.

5. Ion concentration due to induced *electric-field distribution around the smooth nanowire and NTs systems*

In order to study the mechanism of hydrogen generation on the electrode surface, the COMSOL simulation is used. A finite element model was established to calculate the concentration distribution of charged ions in the electrolyte solution under the action of the electric field on the electrode surface. In the model, the electrode with negative potential is immersed in the KOH solution with a pH value of 14. Based on Maxwell equations, the electric field intensity distribution on the surface of NT and smooth NW structure surrounded by electrolyte solution is solved under the condition of negative voltage excitation. Under the action of the electric field, the concentration distribution of hydrogen ions and potassium ions in the solution will change. The H+ and K+ in the calculated region will have different change during this process. Due to the huge difference between the hydrogen ions and potassium ions (nearly 10^{14}), the data were normalized during the simulation. In order to facilitate a fair comparison, firstly we multiply the concentration of hydrogen ion by 10^{14}, then normalize the concentration data of hydrogen ion and potassium ion (the maximum concentration is 1, the minimum concentration is 0), and finally, normalized data was used to draw the comparison graph.

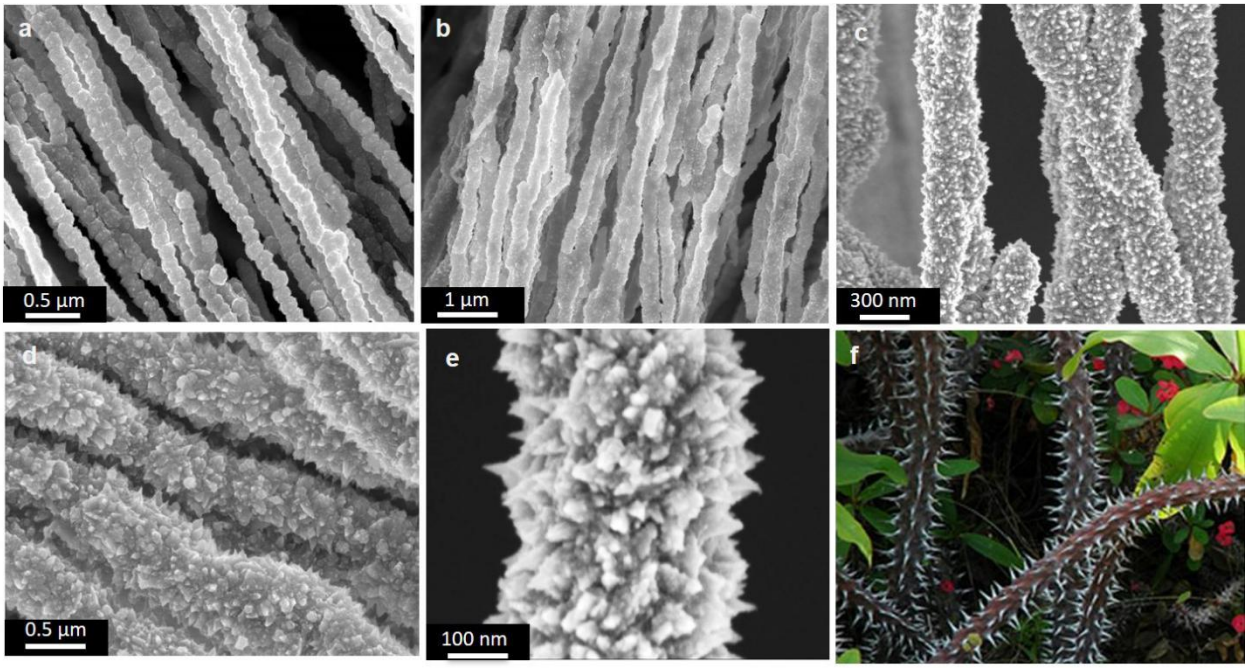

Supplementary Figure 1. SEM image of Ni NTAs obtained at different reaction temperatures (a) 60℃, (b) 70℃, (c) 80℃ (d) 100℃. (e) High magnification SEM image of single Ni-NT prepared at 80℃. (f) Photograph of the crown of thorns.

Supplementary Figure 1. explains the growth mechanism of Ni NTAs. Briefly, at the reaction temperature of 60℃, small spherical Ni nanoparticles can form gradually and then join together, forming chain-like nanostructures with an average diameter of about 200 nm (Figure S1a). With a gradual increase in temperature (70℃), these ferromagnetic particles converge by cold-welding (Figure S1b). When the temperature raised up to 80℃, it will grow up along selective crystalline facets, and we can clearly observe the appearance of sharp nanostructures on the surface of nanowires (Figure S1c and S1e). The representative images show that the obtained products consist of a structure which resembles with a crown of thorns (Figure S1f), that is, some sharp nanotips/nanocones selectively grown on the surface of nanowire, denoting the formation of thorn-shaped nanowire arrays (~350 nm in diameter and ~2mm in length as can be seen in Figure S3). After that, at further elevated temperature (100℃), the thorn-shaped structure was maintained while the nanowire diameter increased up to 500 nm (Figure S1d).

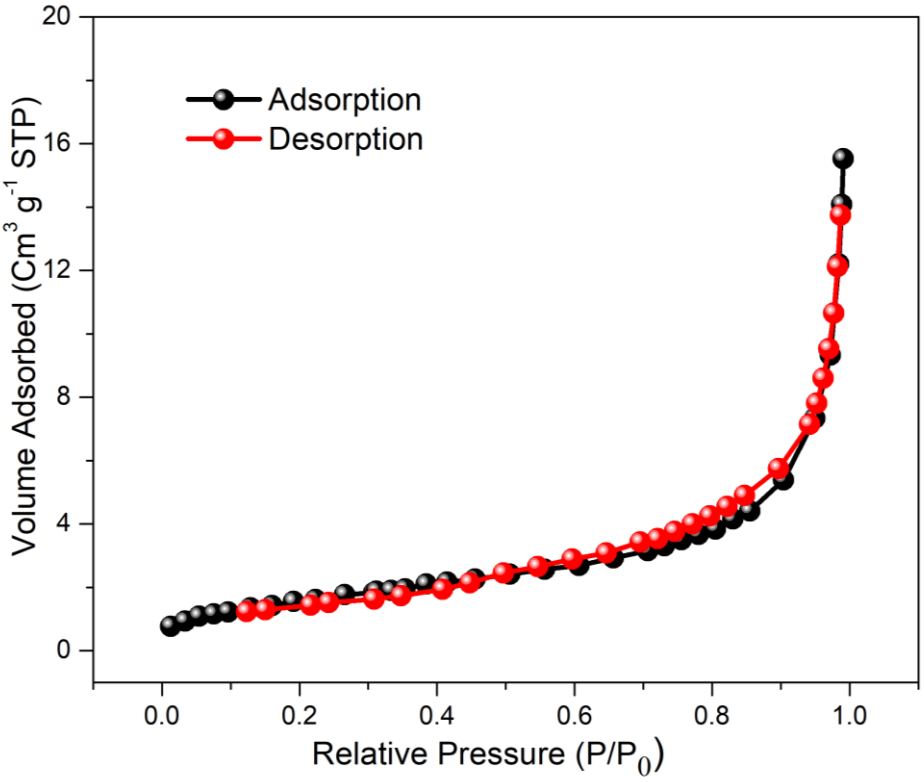

Supplementary Figure 2. N_2 adsorption/desorption isotherms obtained from BET measurement for Pt-Ni NTAs.

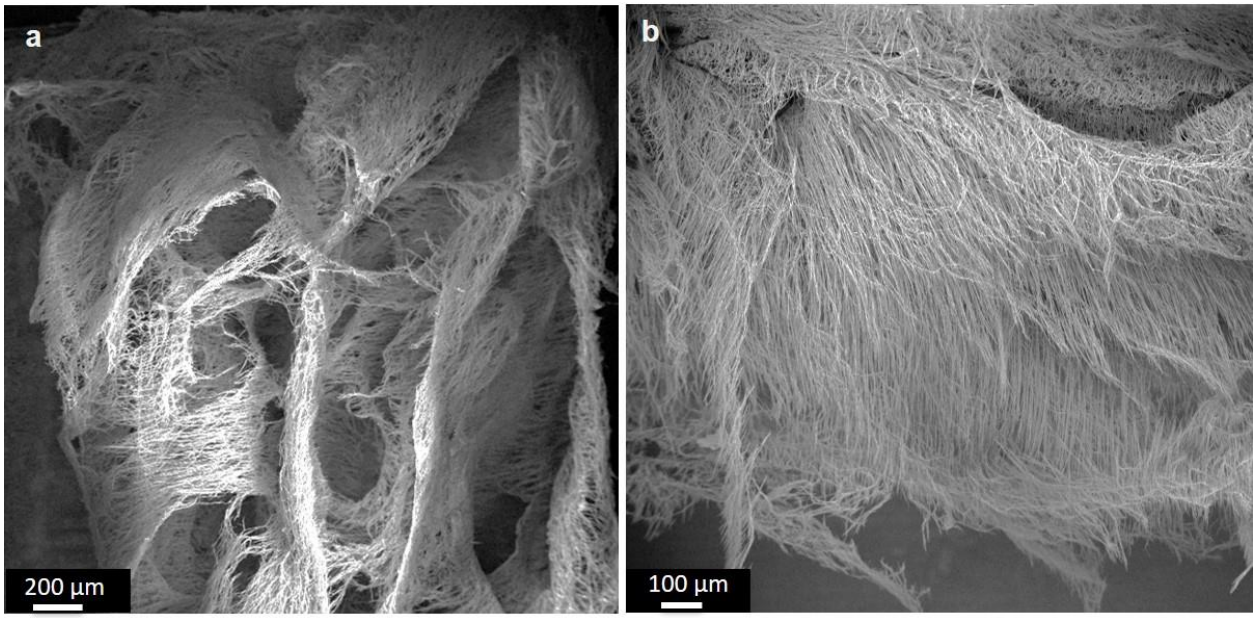

Supplementary Figure 3. (a, b) SEM images of growth of long Ni NTAs on the substrate showing the length of nanowire around 2mm.

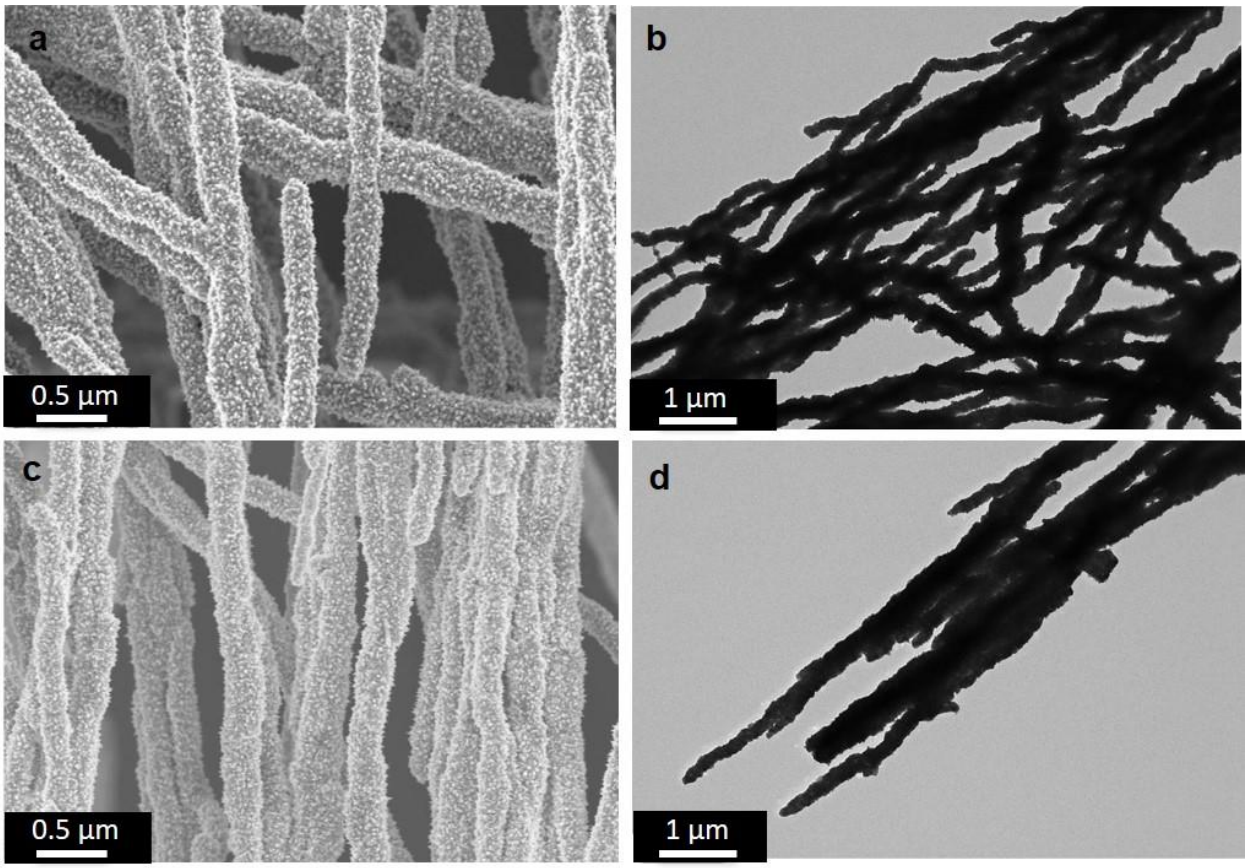

Supplementary Figure 4. (a) SEM image of Ni NTAs. (b) TEM of Ni NTAs. (c) SEM image of Pt-Ni NTAs. (d) TEM image of Pt-Ni NTAs.

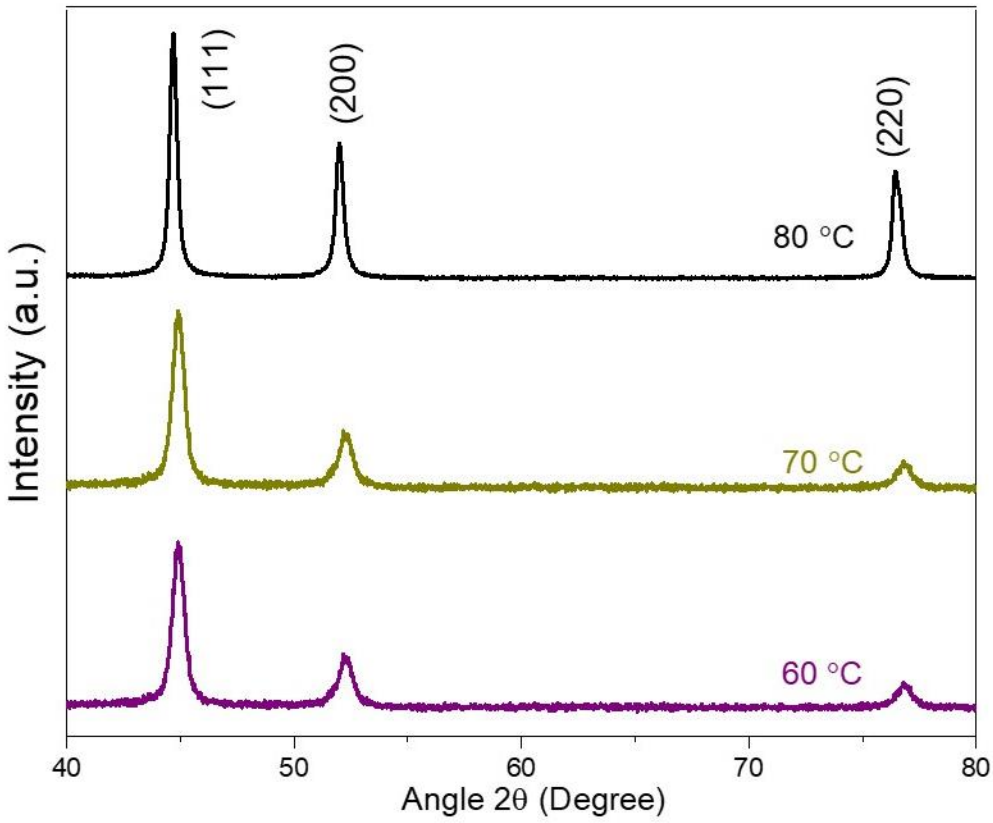

Supplementary Figure 5. XRD patterns of Ni NTAs prepared at different synthetic temperatures

The crystalline phase of pristine Ni NTAs was surveyed with X-ray diffraction using Cu-Kα radiation. The diffraction pattern for Ni NTAs represents sharp peaks at 2θ ~ 44.6°, 52.0° and 76.6°, which well match with the standard JCPS card No. 04-0580. The diffraction peaks can be indexed to fcc Ni structure with a unit cell of a=b=c= 3.524 Å.

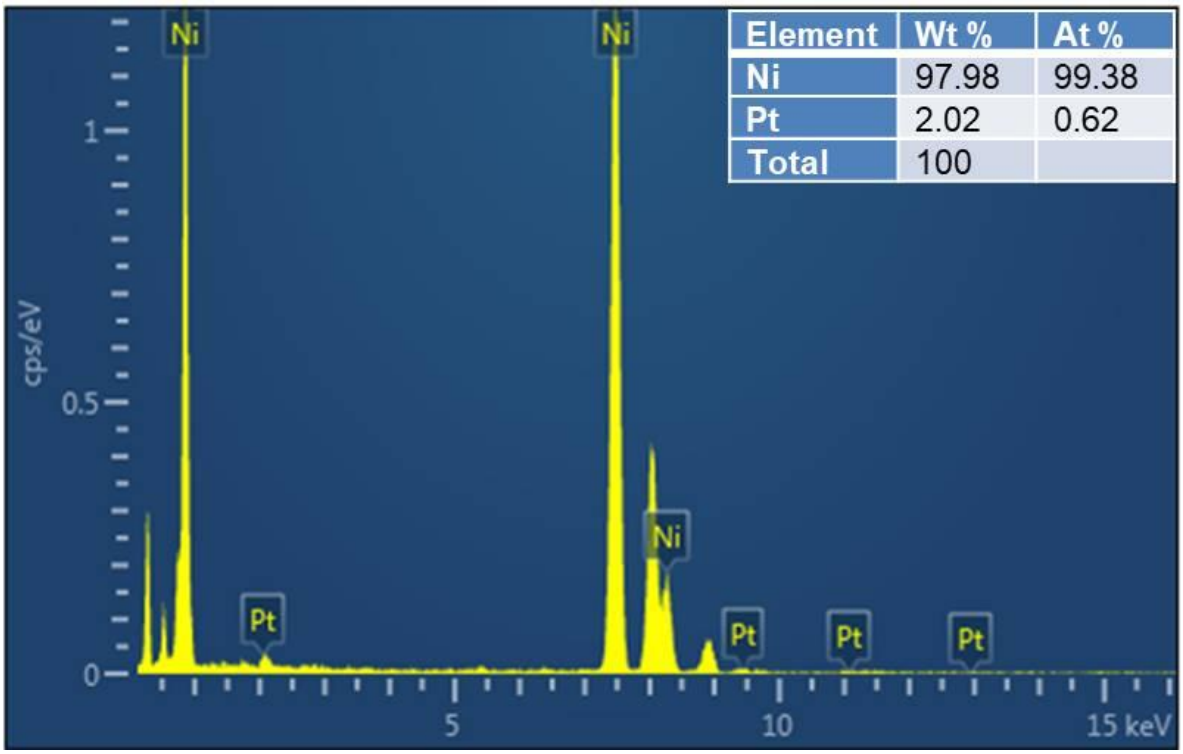

Supplementary Figure 6. A representative EDX spectrum of Pt-Ni NTAs.

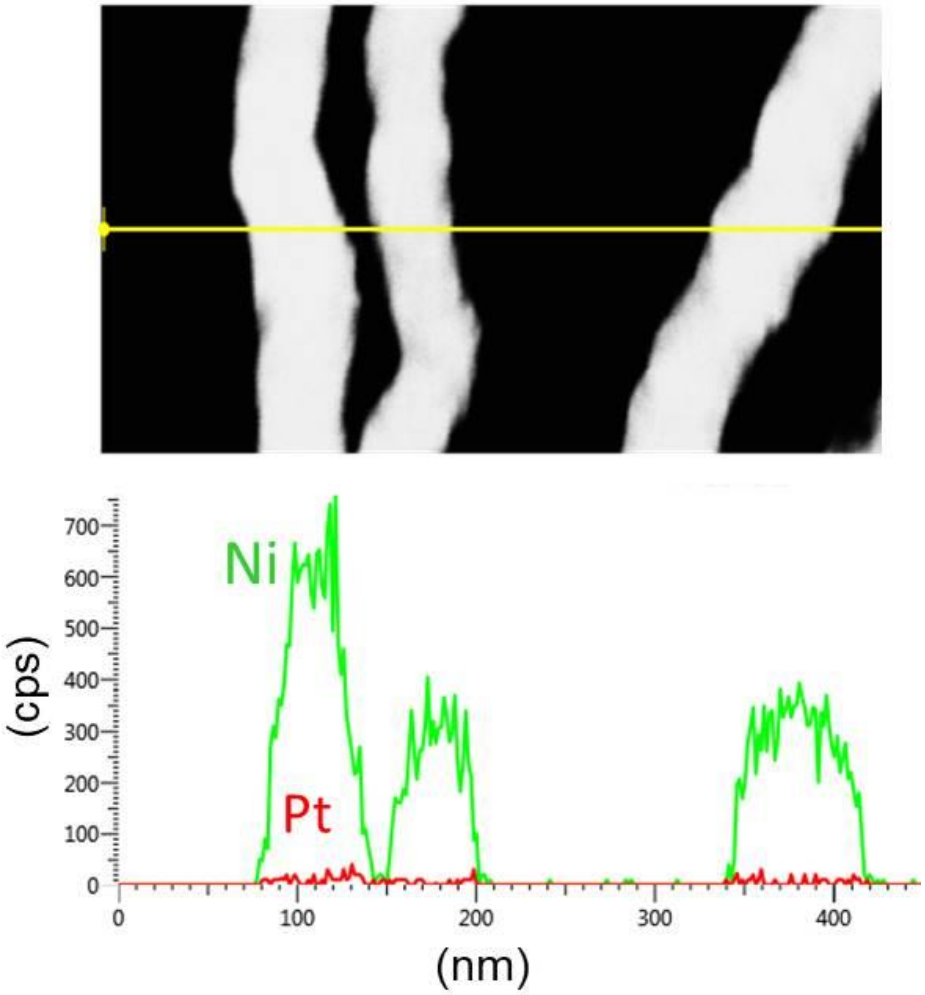

Supplementary Figure 7. The composition analysis of Pt-Ni NTAs characterized by TEM-EDX line scan, where the distribution of present elements Ni and Pt is shown.

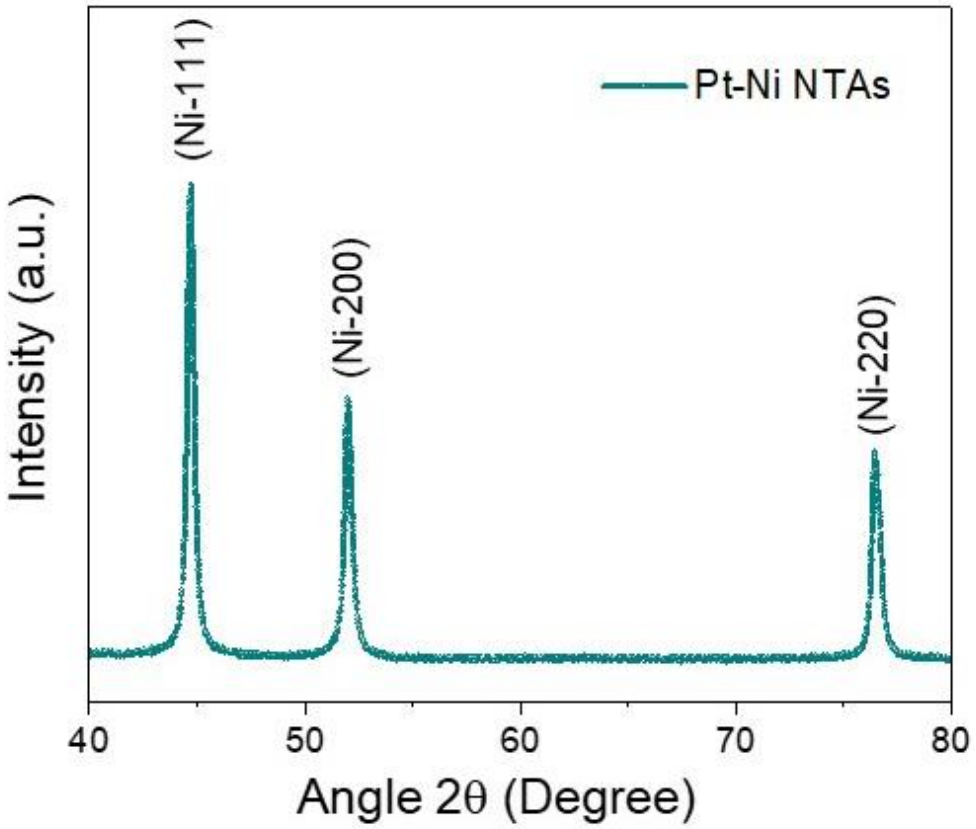

Supplementary Figure 8. XRD pattern for Pt-Ni NTAs.

Supplementary Figure 8 shows the diffractions peaks for Pt-Ni NTAs, but due to a small amount of Pt there was no significant change in XRD pattern.

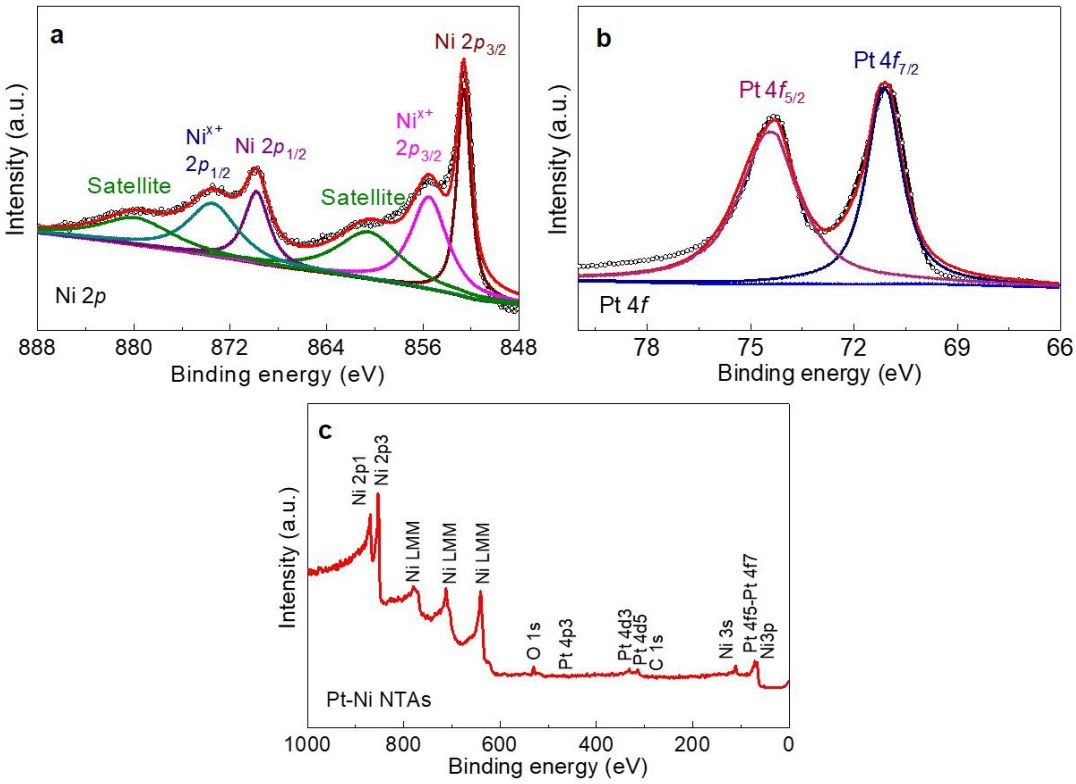

Supplementary Figure 9. XPS analysis for Pt-Ni NTAs (a) High-resolution XPS spectra for Ni 2p. (b) High-resolution XPS spectra for Pt 4f. (c) Survey scan.

High resolution Ni 2p spectrum shows the intense peaks of Ni at 852.5 eV and 870 eV along with the small satellites at 861 eV and 880 eV, which can be assigned to Ni^0, indicating the presence of pure Ni metal[2] (Figure S9a). While, the deconvolution spectrum for Pt comprises two pairs of peaks, corresponding to the dominant Pt^0 metallic atoms in the Pt-Ni NWAs sample (Figure S9b). Figure S9c shows the XPS survey scan for Pt-Ni NTAs electrode, which confirms the existence of both Ni and Pt metals.

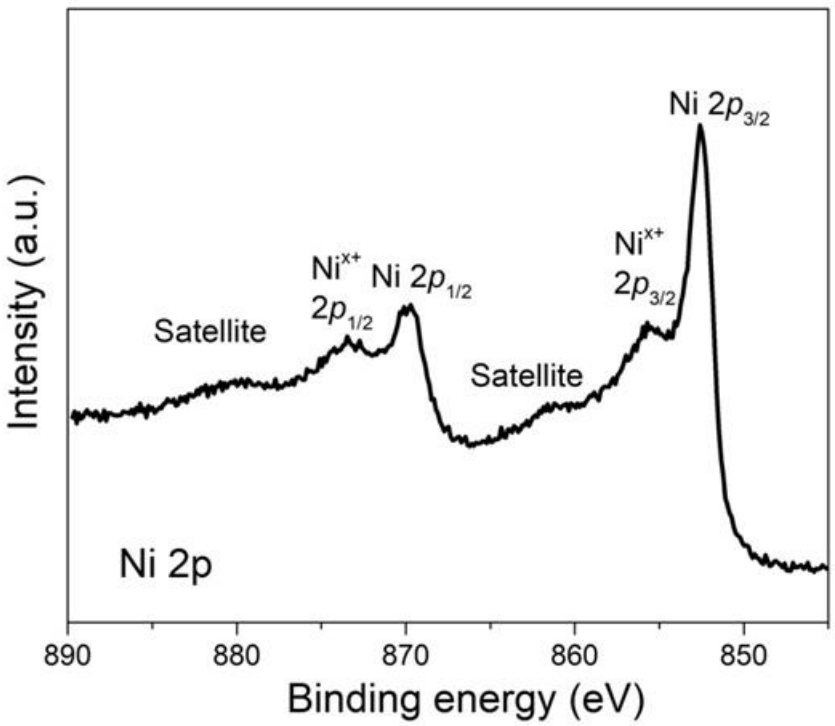

Supplementary Figure 10. XPS spectra for Ni 2p collected from Ni-NTAs.

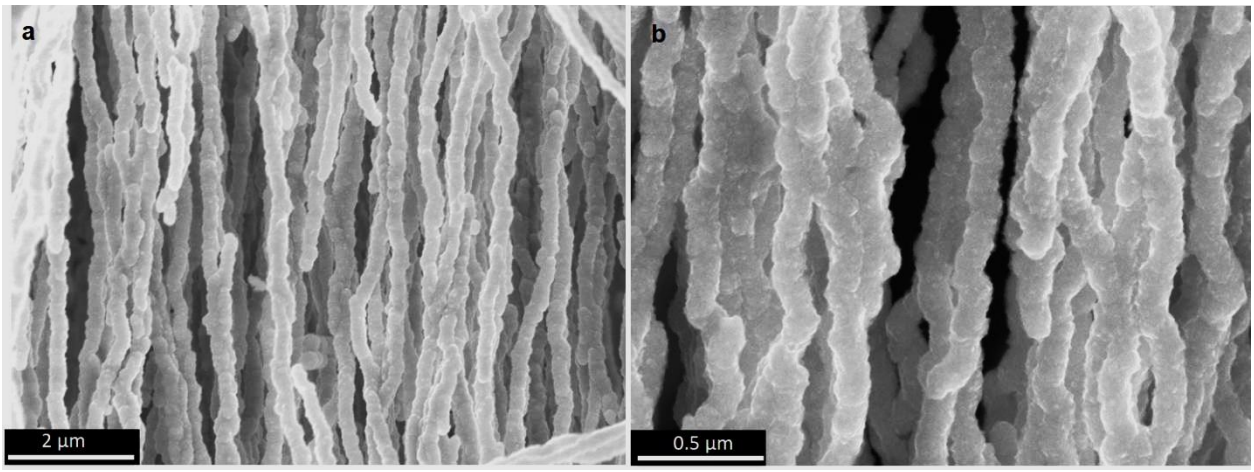

Supplementary Figure 11. (a, b) SEM images of smooth Ni NWAs.

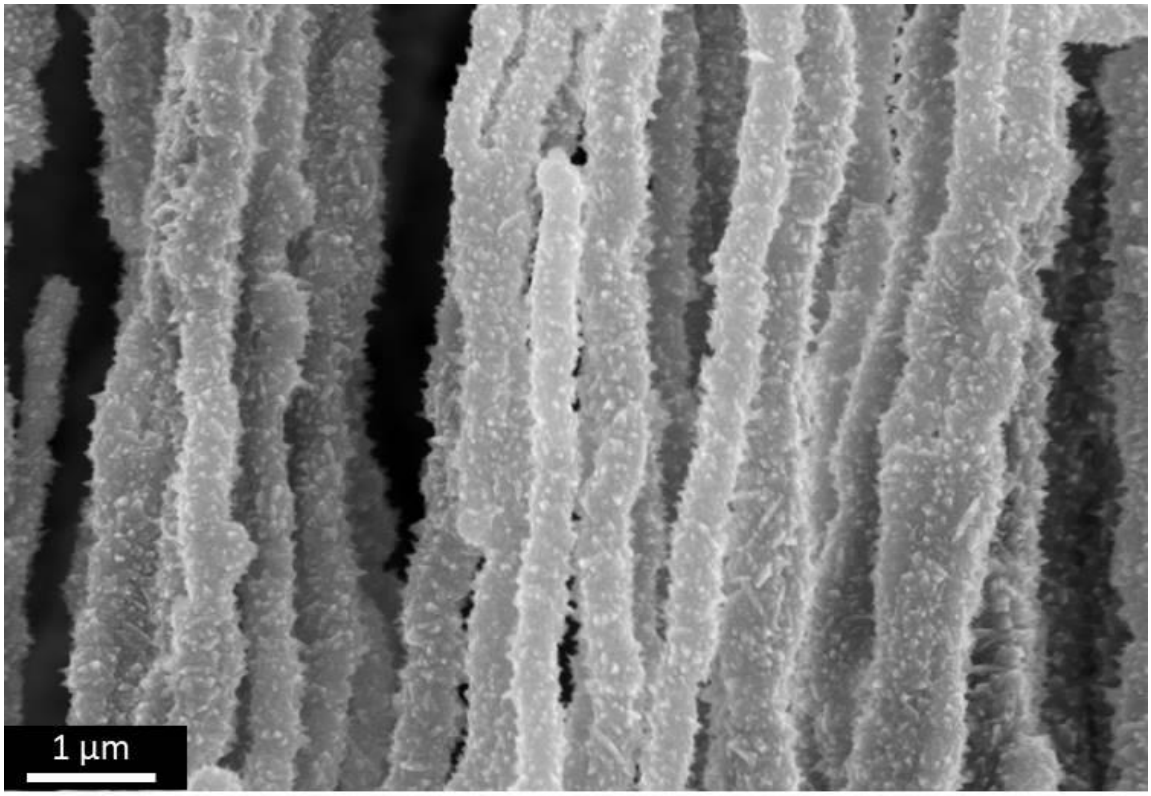

Supplementary Figure 12. SEM micrograph of Pt-Ni NTAs after long-term stability test showing good morphology control after 24 h stability test.

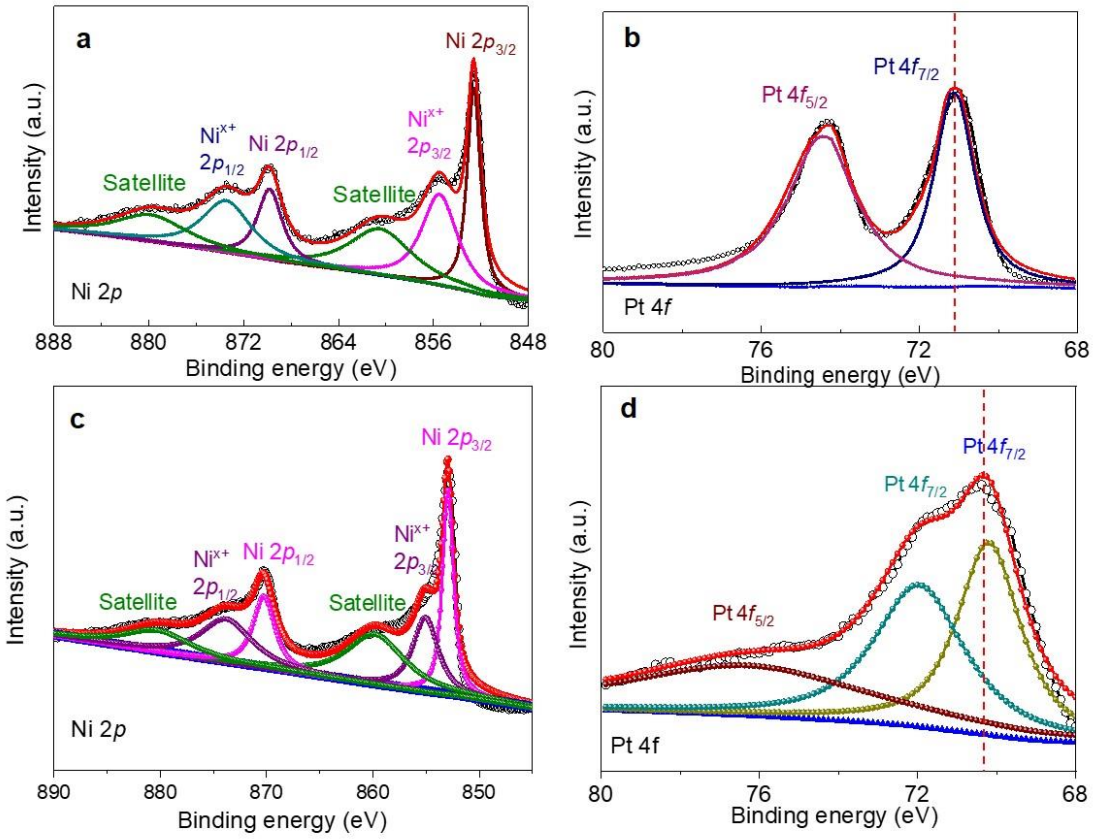

Supplementary Figure 13. XPS spectra of Ni 2p and Pt 4f from Pt-Ni NTAs after 24 h long term stability test (a, b) before stability and (c, d) after stability.

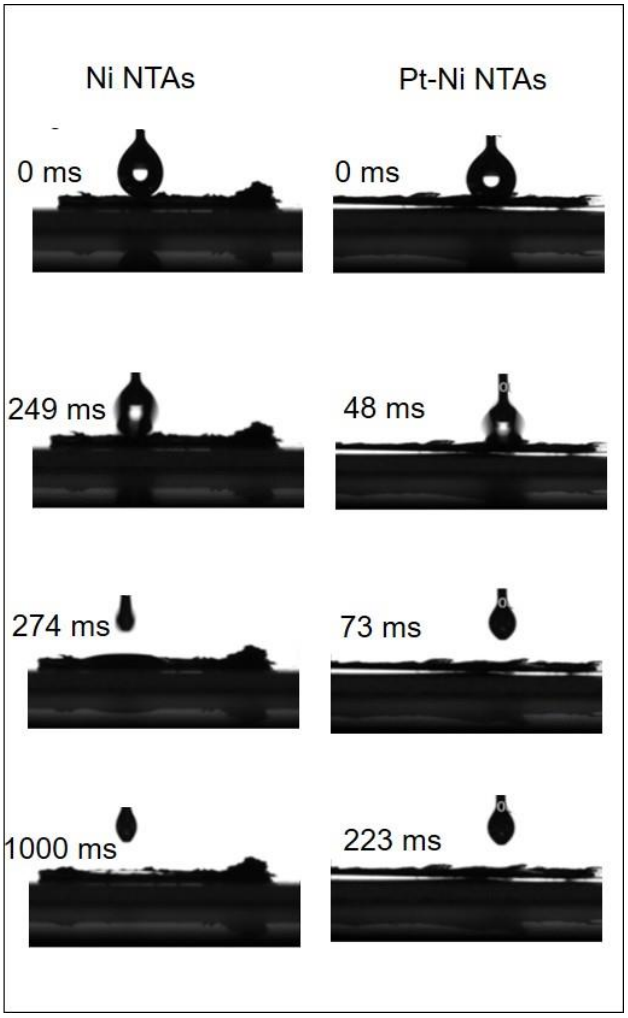

Supplementary Figure 14. Contact angles of a 1.0 M KOH droplet on surfaces of prepared Ni NTAs and Pt-Ni NTAs.

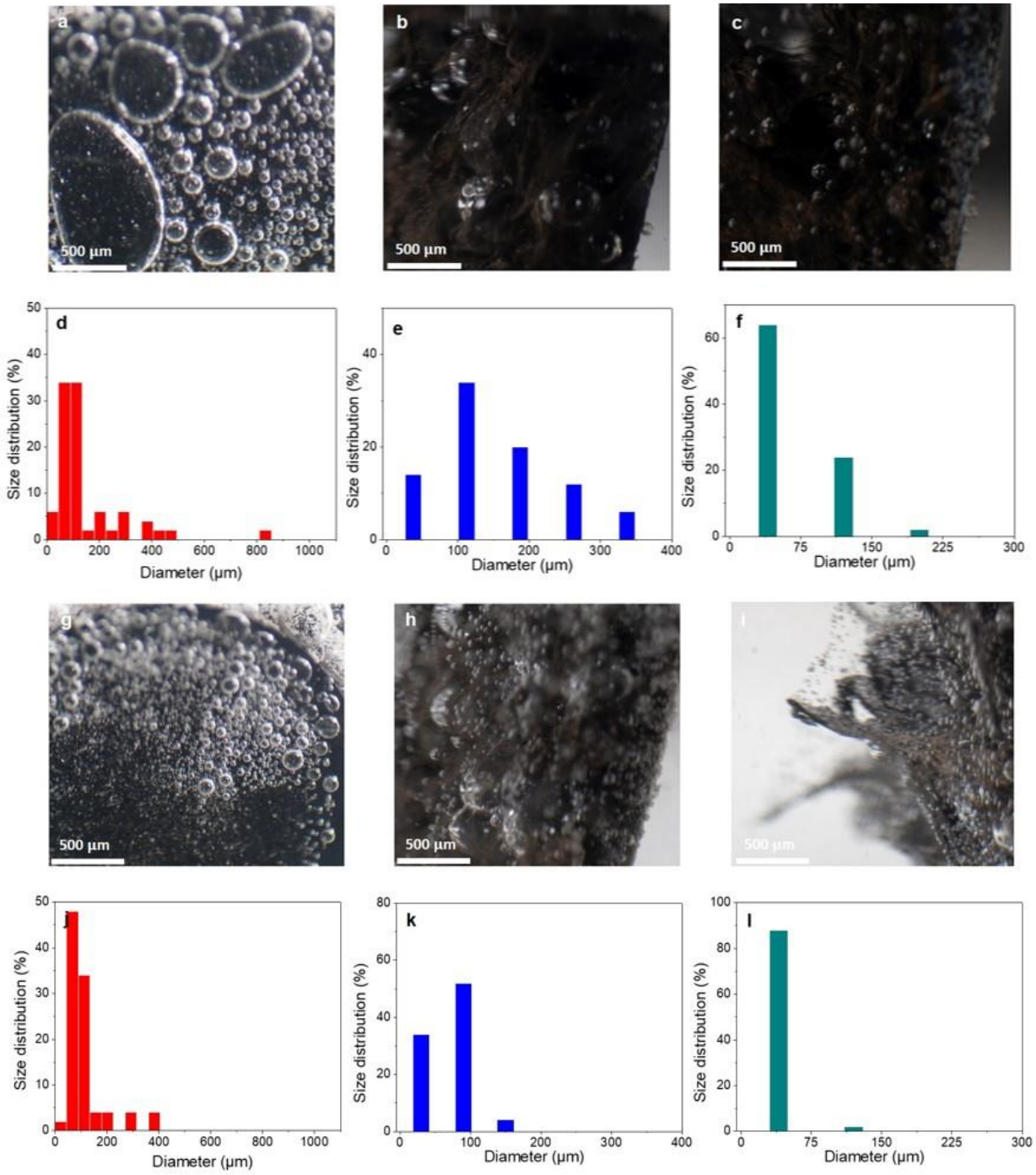

Supplementary Figure 15. Digital photographs demonstrating the hydrogen bubbles on the surface of fabricated electrodes at a current density of 10 mA cm^{-2} for (a) Pt/C, (b) Ni NTAs, and (c) Pt-Ni NTAs. (d-f) The corresponding size distribution statistics of bubble releasing. Hydrogen bubbles on the surface of electrodes at a current density of 200 mA cm^{-2} for (g) Pt/C, (h)Ni NTAs, and (i) Pt-Ni NTAs. (j-l) The corresponding size distribution statistics of bubble releasing on the surface of the electrode. It can be seen that hydrogen bubbles grow to very large size for Pt/C (*i.e.* larger than 400 µm) and Ni-

NTAs (*i.e.* larger than 150 µm) at low and high current densities while leaving easily from the surface of Pt-Ni NTAs (*i.e.* smaller than 100 µm).

The morphological features of Pt-Ni NTAs provide the intriguing possibility of displacing as-generated gas bubbles from the electrode surface, a parameter simply known as superaerophobicity. Superaerophobic behavior would allow fast mass transfer and constant exposure of catalytic active sites to the surrounding electrolyte. This concludes, that fabricated electrode with a high degree of surface roughness not only generates a strong capillary force to pump liquid but also minimize the interfacial adhesion to improve gas bubble release[3].

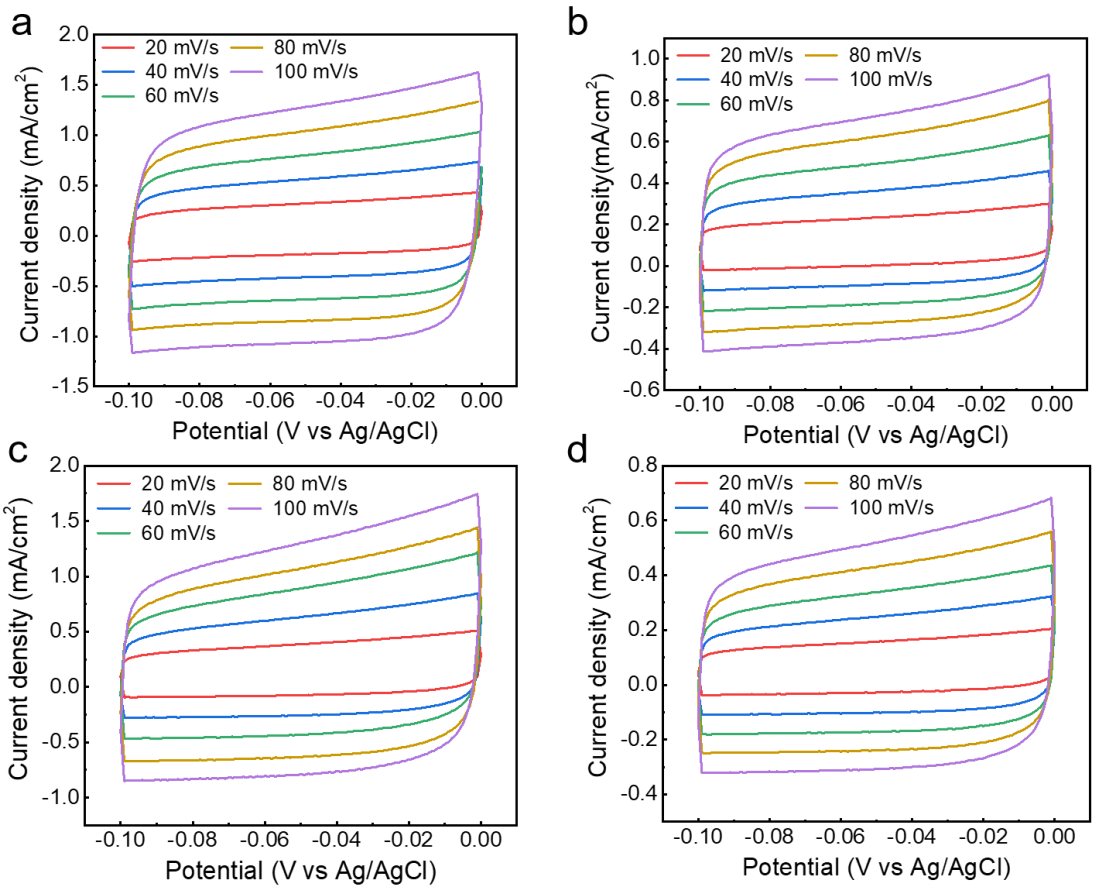

Supplementary Figure 16. Cyclic voltammetry curves of the fabricated catalysts at different scan rates of (a) Pt-Ni NTAs, (b) Pt-Ni NWAs, (c) Ni NTAs and (d) Ni NWAs

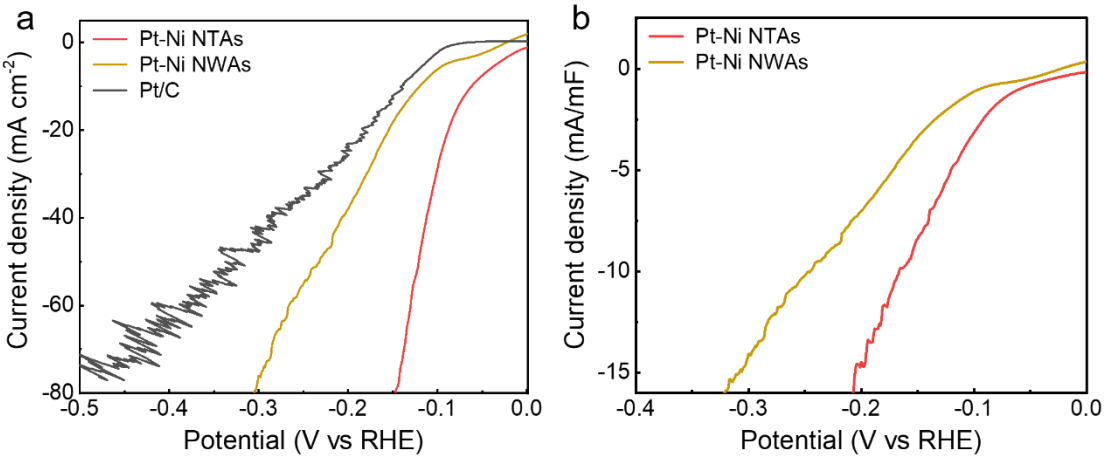

Supplementary Figure 17. a) Polarization curves for Pt-Ni NTAs, Pt-Ni NWAs and Pt/C under 0.05 M H_2SO_4 solution and b) C_{dl} normalized polarization curves for Pt-Ni NTAs and Pt-Ni NWAs.

.

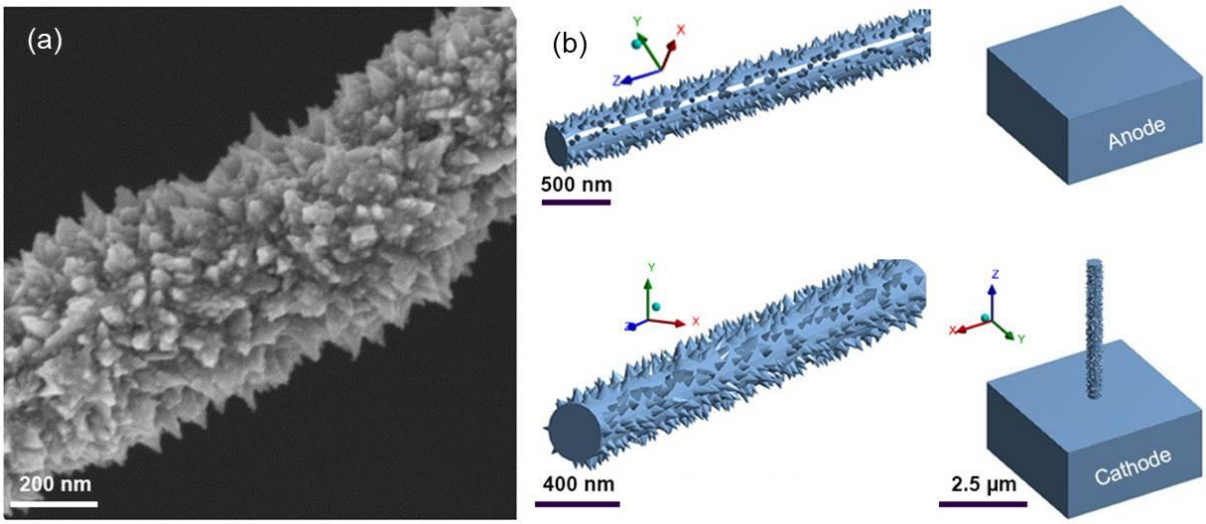

Supplementary Figure 18. a) SEM micrograph of Ni NTs. b) The NW model and electrochemical system in the 3D view, the NW with NTs is attached to the cathode, counter positioning with the anode on top. The KOH electrolyte is transparent between the two electrodes.

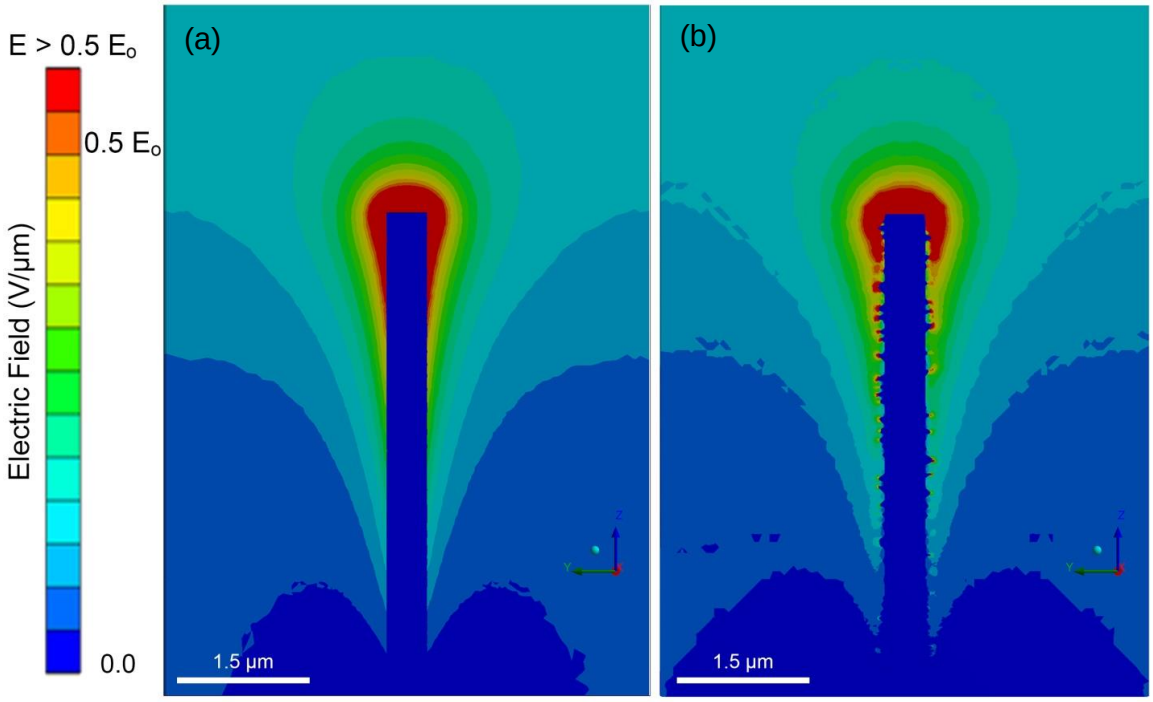

Supplementary Figure 19. The 2D distribution of Electric field surrounding the nanowire models at the Z-Y cross-section plan, where (a) smooth NW (control case), (b) NW decorated with NTs. The smooth NW has a stronger field and is sensitive to its surrounding. The Electric field distribution of the coated and model NWs are very similar and are more stable to the environment. Changing of coating thickness and resistivity within our designated range has little effect on the Electric field. E_0 is the reference Electric field strength between the electrodes.

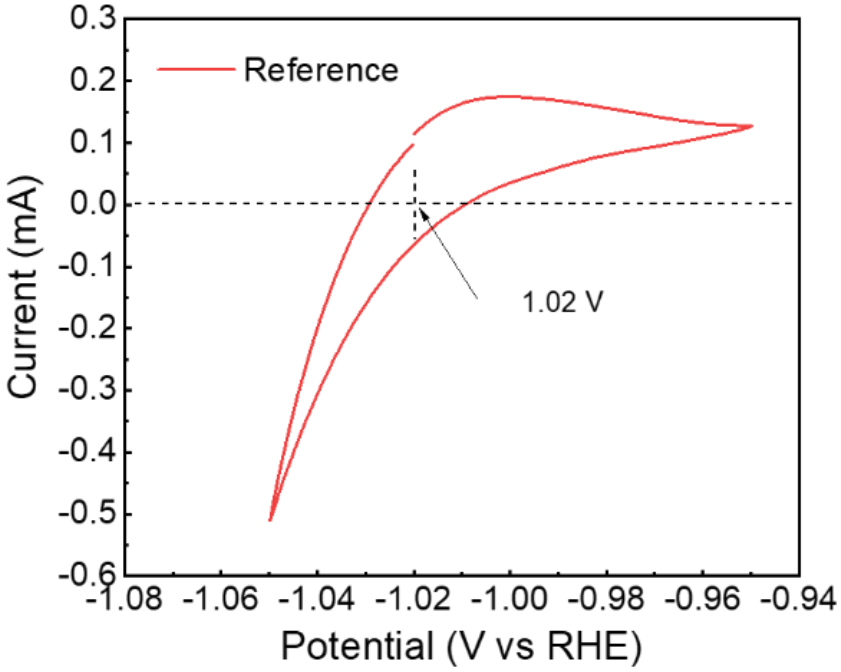

Supplementary Figure 20. Calibration of the used Ag/AgCl reference electrode.

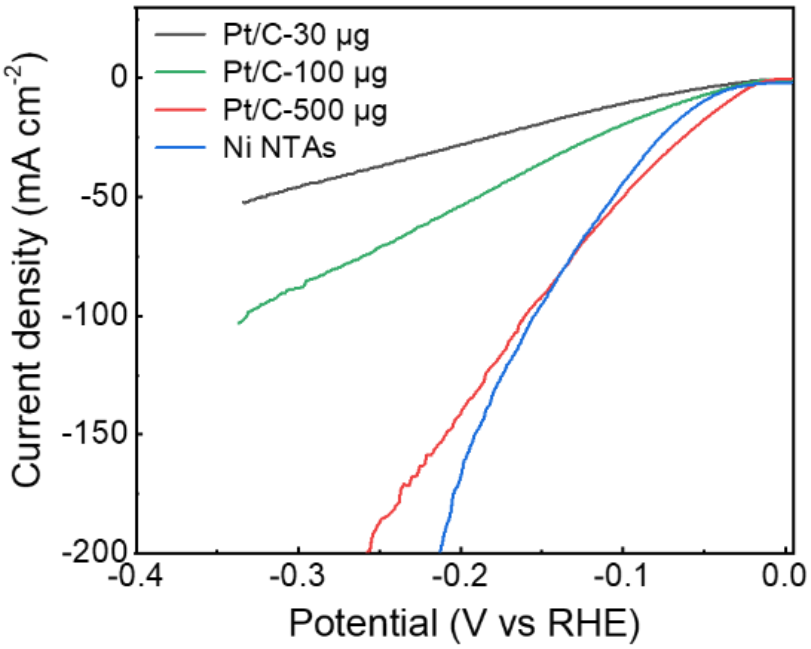

Supplementary Figure 21. Polarization curves of Pt/C catalysts with different mass loading and Ni NTAs.

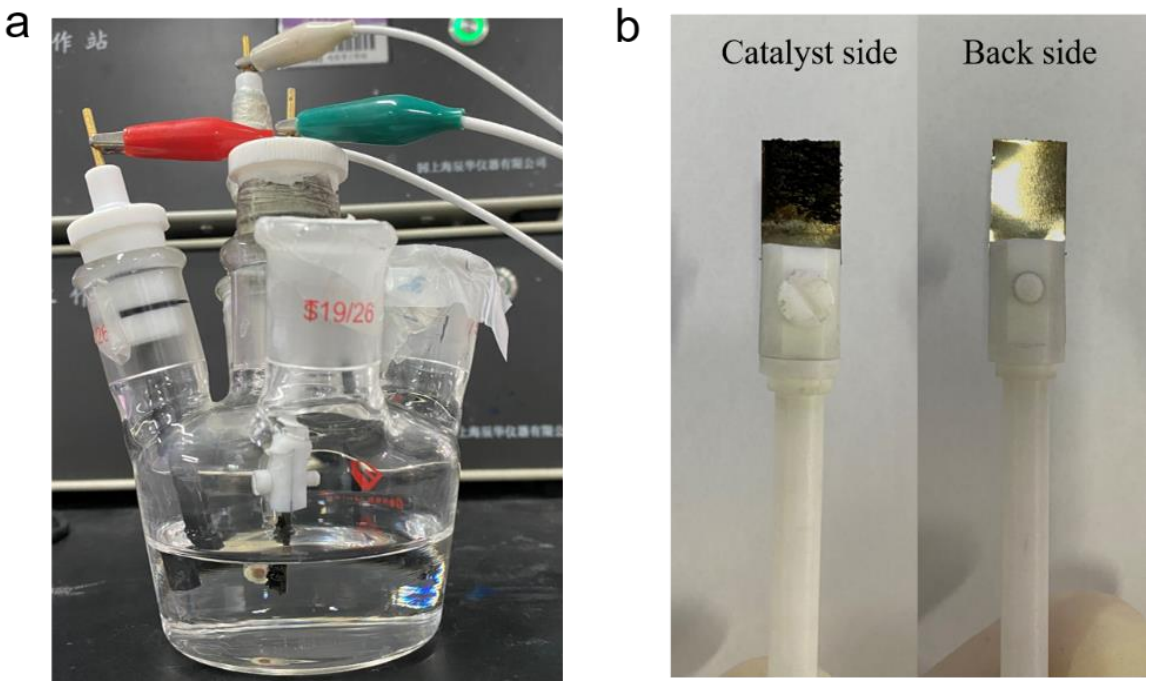

Supplementary Figure 22.. a) Optical image of the used electrolyzer (Gaoss Union Co.) and b) different sides of nanowire arrays catalytic electrode.

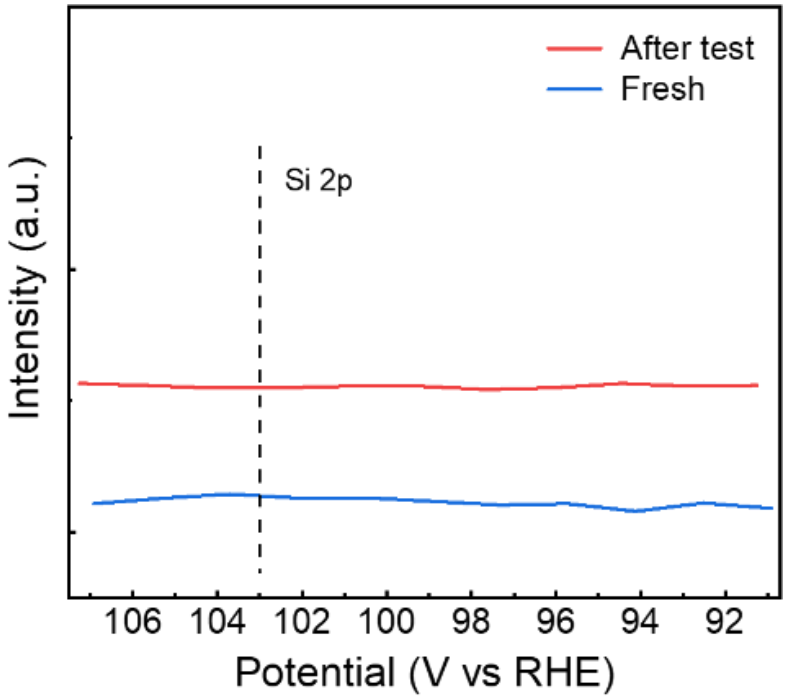

Supplementary Figure 23. XPS spectrum of Si 2p after stability test, and no obvious Si signal was detected, indicating not glassware corrosion by alkaline.

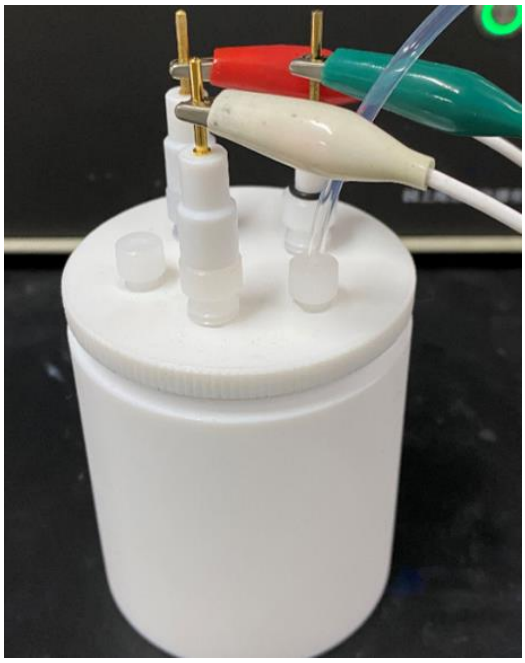

Supplementary Figure 24. Optical image of the improved set-up with PTFE electrolyzer and N_2 bubbling for stability test.

Supplementary Table 1. The elemental concentration of Ni and Pt in the prepared electrode obtained from ICP.

Ni (mg/L)	Pt (mg/L)	Calculated Ni: Pt (atomic ratio)
155.7	1.005	99.8:0.2

Supplementary Table 2. Comparison of Pt-Ni NTAs catalytic performance based on the geometric surface area with some recently reported HER electrocatalysts in alkaline medium.

Catalyst	Mass loading	Current density (mA cm^{-2})	Overpotential at corresponding current density (mV)	Tafel slope (mV dec^{-1})	References
Pt-Ni NTAs	(Pt) 0.016mg cm^{-2}	10 100 200	23 56 71	38	This Work
Ni NTAs	1.5 mg cm^{-2}	10 100 200	51 155 213	57	This Work
RuCoP	0.3	10 100	23 105	37	Energy Environ. Sci. 11, (2018), 1819.
Pt_3Ni_2-NWs-S/C	(Pt) 0.015 mg cm^{-2}	10 35	42 ~100	/	Nature Comm. 8, (2017)14580.
Ru/NG-750	/	10	8	30	ACS Appl. Mater. Interfaces 9, 3785–3791 (2017)
Mo_2N-Mo_2C/HGr-3	0.337 mg cm^{-2}	10 100	154 ~400	68	Adv. Mater. 30, (2018) 1704156.
Co-substituted Ru	0.153 mg cm^{-2}	10	13	29	Nat. Comm. 9, 4958 (2018)
Pt-Ni ASs	(Pt) 0.017 mg cm^{-2}	10 50	27.7 ~70	27	Adv. Mater. 30 (2018) 1801741.
Single atom Co/PCN	/	10 50	89 ~105	52	Nature catalysis 2, (2019) 134-141.
PtNi alloy nano multipods	(Pt) 0.008 mg cm^{-2}	22	70	78	Nat. Comm. 8, (2017), 15131.
NiO_x/ Pt_3Ni_3-NWs	(Pt) 0.015 mg cm^{-2}	10	40	/	Angew. Chem. Int. Ed. 55 (2016), 12859.
Pt NWs/SL-$Ni(OH)_2$	(Pt) 0.016 mg cm^{-2}	4 30	85.5 ~120	/	Nat. Comm. 6, (2015), 6430.
Pt_3Ni frames/$Ni(OH)_2$/C	(Pt) ~0.014 mg cm^{-2}	4	~60	/	Science, 343 (2014) 1339.
N-$NiCo_2S_4$	/	10 100	28 ~130	37	Nature Comm. 9, (2018), 1425.

Ni(Cu)/NF	/	10 100	27 ~110	33.3	Small, 14, (2018) 1704137.
Ru@C_2N	0.285 mg cm^{-2}	10 30	17 ~28	38	Nature Nanotechnol. 12, (2017), 441.
Co $(OH)_2$/Pt (111)	/	10	~248	/	Nature Mater. 11, (2012), 550.
CoN_x/C	2 mg cm^{-2}	10	170	75	Nature Comm. 6, (2015), 7992.
$NiCo_2S_4$/Ni foam	/	10 100	65 ~210	84.5	Nano Energy, 24, (2016), 139.
$CoMoS_x$	50 μg cm^{-2}	5	~185	/	Nature Mater. 15, (2016), 197.
MoCx nano-octahedrons	0.8 mg cm^{-2}	10 60	151 ~235	59	Nature Comm. 6, (2015), 6512.
$NiFeO_x$/CFP	1.6 mg cm^{-2}	10 100	88 ~210	150	Nature Comm. 6, (2015), 7261.
NiO/Ni-CNT	0.28 mg cm^{-2}	10 20	~86 ~115	82	Nature Comm. 5, (2014), 4695.
np-CuTi	/	10 30	~47 ~85	110	Nature Comm. 6, (2015), 6567.
NiSe@CoP NWs/NF	/	10 50	91 ~200	55	Catl. Sci. Technol., 8, (2018), 128.

Supplementary Table 3. Fitting results of the Rct for different catalysts.

Samples	Rs (Ω)	Charge transfer resistance Rct (Ω)
Pt-Ni NTAs	0.77	0.22
Pt-Ni NWAs	1.01	0.67
Ni NTAs	0.85	3.8
Ni NWAs	1.24	6.4

Supplementary Table 4. The statistics on NT geometrical parameters.

	Simulation Model		Observation from SEM	
Items	**mean**	**Standard Deviation**	**mean**	**Standard Deviation**
NT height (nm)	67.5	5.40	70.0	4.25
NT base diameter (nm)	60.0	8.60	50.0	6.99
NT slant angle (deg)	15.0	6.70	12.3	7.87
NT tip angle (deg)	45.0	8.60	47.0	11.67
NT number density (μm^{-2})	140	-	138	-

References

1. H. Jiang, Z. Hou and Y. Luo, *Angew. Chem. Int. Ed.*, 2017, **56**, 15617 –15621.
2. Y.-Y. Chen, Y. Zhang, X. Zhang, T. Tang, H. Luo, S. Niu, Z.-H. Dai, L.-J. Wan and J.-S. Hu, *Advanced Materials*, 2017, **29**, 1703311.
3. Y. Luo, L. Tang, U. Khan, Q. Yu, H.-M. Cheng, X. Zou and B. Liu, *Nature Communications*, 2019, **10**, 269.